GEOLOGY | THE GEOLOGICAL SOCIETY OF AMERICA®

https://doi.org/10.1130/G48881.1

Manuscript received 29 January 2021
Revised manuscript received 20 March 2021
Manuscript accepted 24 March 2021

Mass balance controls on sediment scour and bedrock erosion in waterfall plunge pools

Joel S. Scheingross[1]* and Michael P. Lamb[2]
[1]Department of Geological Sciences and Engineering, University of Nevada Reno, Reno, Nevada 89557, USA
[2]Division of Geological and Planetary Sciences, California Institute of Technology, Pasadena, California 91125, USA

ABSTRACT

Waterfall plunge pools experience cycles of sediment aggradation and scour that modulate bedrock erosion, habitat availability, and hazard potential. We calculate sediment flux divergence to evaluate the conditions under which pools deposit and scour sediment by comparing the sediment transport capacities of waterfall plunge pools (Q_{sc_pool}) and their adjacent river reaches (Q_{sc_river}). Results show that pools fill with sediment at low river discharge because the waterfall jet is not strong enough to transport the supplied sediment load out of the pool. As discharge increases, the waterfall jet strengthens, allowing pools to transport sediment at greater rates than in adjacent river reaches. This causes sediment scour from pools and bar building at the downstream pool boundary. While pools may be partially emptied of sediment at modest discharge, floods with recurrence intervals >10 yr are typically required for pools to scour to bedrock. These results allow new constraints on paleodischarge estimates made from sediment deposited in plunge pool bars and suggest that bedrock erosion at waterfalls with plunge pools occurs during larger floods than in river reaches lacking waterfalls.

INTRODUCTION

Sediment fill and scour cycles in waterfall plunge pools can erode bedrock (e.g., Scheingross and Lamb, 2017), modify habitat (e.g., Magoulick and Kobza, 2003), and form deposits that preserve paleoclimate information (e.g., Nott and Price, 1994). For example, plunge pool erosion can drive waterfall retreat (Gilbert, 1890) but requires that pools scour to their bedrock floors because deposited sediment armors the bed, preventing incision (Lamb et al., 2007; Scheingross and Lamb, 2017). Deep pools are refuge for fish (e.g., Nielsen et al., 1994), and when pools fill with sediment, this habitat is lost and the pools instead create a hazard because sediment fills can liquefy by plunging jets, forming debris flows (e.g., Griffiths et al., 2004). Bars formed at the downstream boundary of plunge pools can be long lived and are used in paleodischarge and paleoclimate estimates (e.g., Carling and Grodek, 1994; Nott et al., 1996).

Most previous plunge pool studies have focused on sediment motion thresholds and the controls of plunge pool depth under clear water flow (zero sediment supply), as occurs below dams (e.g., Mason and Arumugam, 1985; Stein et al., 1993; Pagliara et al., 2006). Such a theory cannot explain sediment fill and evacuation in natural pools where sediment is supplied from upstream. Instead, mass balance dictates that pools fill when the upstream sediment supply exceeds the ability of the pool to transport that sediment, and pools scour when the sediment supply is less than the pool transport capacity. Plunge pool sediment transport capacity theory has only recently been developed (Scheingross and Lamb, 2016), and the relative transport capacities of plunge pools and rivers have not been compared.

Sediment deposited below waterfalls suggests that plunge pools respond to different transport thresholds than their adjacent river reaches (Carling, 1995). Waterfall plunge pools typically have bars at their downstream boundary that are coarser than the adjacent riverbed material, yet the pools are commonly filled with finer sediment than the adjacent riverbed (Fig. 1; Fig. S1 in the Supplemental Material[1]) (e.g., Carling, 1989, 1995). The juxtaposition of fine-grained pool deposits and coarse-grained bars, neither of which match the riverbed material, suggests that plunge pools likely experience sediment transport at different times than adjacent river reaches. Different thresholds for bedrock erosion in pools relative to rivers can create spatially variable erosion rates along rivers, which can alter knickpoint response to climatic and tectonic perturbations (DiBiase et al., 2015; Scheingross et al., 2020).

We coupled plunge pool and river sediment transport theory to predict when plunge pools transition from sediment aggradation to scour. We built on the previously developed plunge pool sediment transport capacity theory (Scheingross and Lamb, 2016) by using it to model fill and scour cycles in plunge pools, and by comparing the results to field data.

THEORY AND METHODS

By mass balance, plunge pools aggrade when the volumetric sediment flux (L^3/T, where L and T represent units of length and time, respectively) into the pool (Q_{s_river}) exceeds the flux out (Q_{s_pool}) (Fig. 2A). We hypothesize this occurs at low water discharge because the waterfall jet diffuses within the pool, limiting sediment export from the pool (Scheingross and Lamb, 2016). In contrast, during high discharge, the falling jet impinges on the pool floor, allowing sediment transport in the pool to exceed that of the adjacent channel reaches and resulting in sediment scour and potentially bedrock erosion (Fig. 2A) (e.g., Keller, 1971; Lisle, 1979). Furthermore, when Q_{s_pool} exceeds the river transport capacity downstream, bars form at the pool boundary to achieve mass balance.

*E-mail: jscheingross@unr.edu

[1]Supplemental Material. Methods, Tables S1 and S2 (data), and Figures S1–S4. Please visit https://doi.org/10.1130/GEOL.S.14524266 to access the supplemental material, and contact editing@geosociety.org with any questions.

CITATION: Scheingross, J.S., and Lamb, M.P., 2021, Mass balance controls on sediment scour and bedrock erosion in waterfall plunge pools: Geology, v. 49, p. , https://doi.org/10.1130/G48881.1

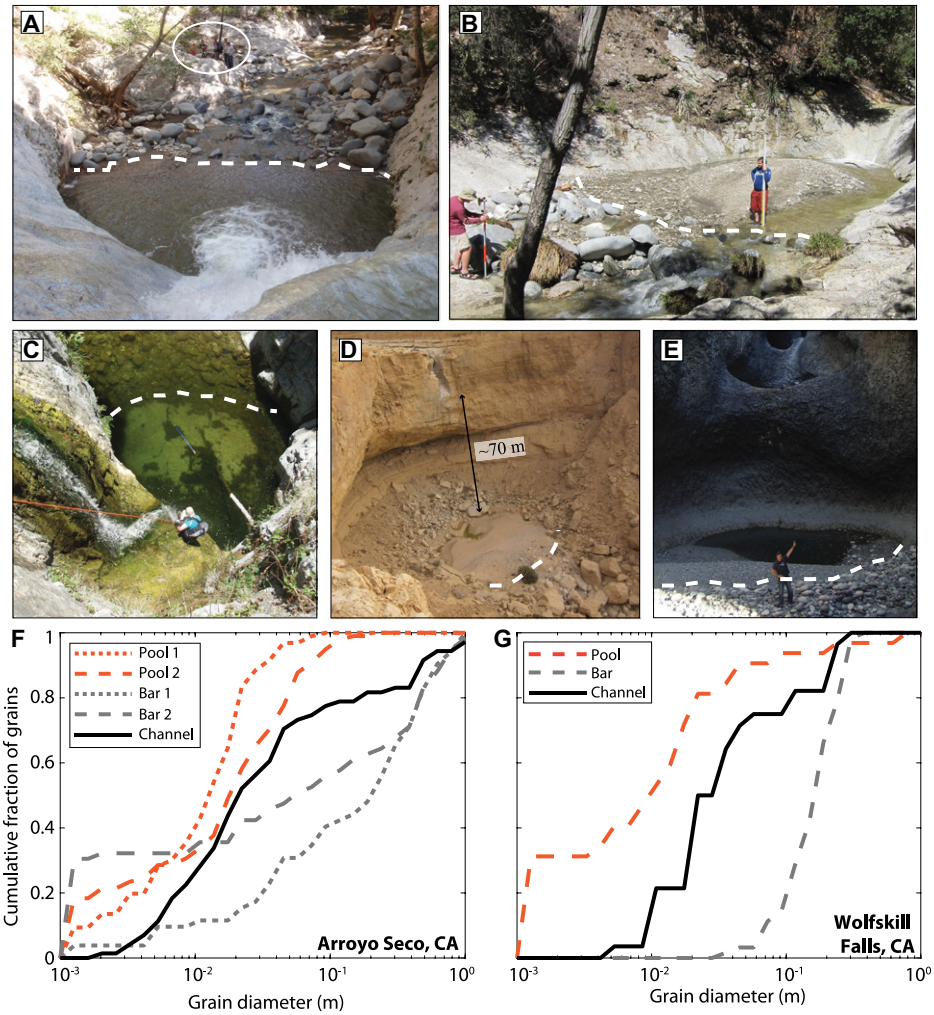

Figure 1. (A–E) Plunge pools with fine-grained fills and coarse-grained bars in the San Gabriel Mountains, California, USA (A–C), Nahal Heimar, Israel (D), and Siete Tazas, Chile (E). White dashed lines indicates the boundary between relatively fine sediment deposited in the plunge pool and coarse sediment deposited in the bar immediately downstream of the plunge pool. Note the presence of people (circled) in A for scale. (F,G) Grain-size distribution for pools in the San Gabriel Mountains (Table S2 [see footnote 1]). CA—California. Photos in C and D were provided by B. Pelletier and G. Vergara Muñoz, respectively.

To explore this hypothesis, we modeled pool aggradation-scour cycles with an Exner equation:

$$\frac{d\eta}{dt} = -\frac{1}{(1-p)}\frac{Q_{s\_pool} - Q_{s\_river}}{A_{pool}}, \quad (1)$$

where η is the elevation of the sediment bed in the pool, t is time, A_{pool} is the pool plan-view area, and $p = 0.35$ is sediment porosity. For simplicity, our model uses a single characteristic particle size for grain-size mixtures (e.g., median size), which is typical in sediment transport studies (e.g., Buffington and Montgomery, 1997). We do not expect that size-selective transport, which can be accounted for by explicit modeling of grain-size mixtures (e.g., Parker, 1990; Wilcock and Crowe, 2003), changes our primary findings (see the Supplemental Material). Bedrock rivers commonly evolve to transport the imposed sediment supply at transport capacity (Finnegan et al., 2007; Phillips and Jerolmack, 2016; Pfeiffer et al., 2017); therefore, we assumed transport-limited conditions, and set Q_{s_pool} and Q_{s_river} equal to the plunge pool (Q_{sc_pool}) and river (Q_{sc_river}) volumetric sediment transport capacity, respectively. The transition between sediment aggradation and scour in plunge pools (i.e., $d\eta/dt = 0$) occurs when $Q_{s\_pool} = Q_{s\_river}$.

We calculated plunge pool sediment transport capacity following Scheingross and Lamb (2016). This model evaluates Q_{sc_pool} using the waterfall height, plunge pool geometry, sediment size, and the flow hydraulics and geometry of the adjacent river reach (see the Supplemental Material). Because the critical Shields stress for incipient motion in plunge pools, τ_{*c_pool}, is not well defined, we allowed it to vary from 0.03 to 0.06. We calculated the total river sediment transport capacity (the sum of the bedload and suspended load capacities), Q_{sc_river}, following Lamb et al. (2008a) (see the Supplemental Material). We set river channel critical Shields stress to $\tau_{*c\_river} = 0.15S^{0.25}$, where S is bed slope (Lamb et al., 2008b), and assumed steady, uniform flow (see the Supplemental Material).

We solved for the discharge at which $d\eta/dt = 0$ numerically by calculating Q_{sc_river} and Q_{sc_pool} across a range of discharges and found the discharge at which $Q_{sc\_river} = Q_{sc\_pool}$ (see the Supplemental Material). We evaluated our theory using a reference site, Middle Switzer Falls, California, USA (Table S1 in the Supplemental Material), which is part of a database of 75 waterfalls surveyed by Scheingross and Lamb (2016). Middle Switzer Falls has characteristic values of a 3-m-tall waterfall, 4 m pool radius, 3.5% channel slope above and below the waterfall, 5 m channel width, and median river particle size of 2.1 cm (Scheingross and Lamb, 2016). We estimated that the bedrock pool depth was equal to the pool radius (4 m) (see the Supplemental Material).

RESULTS

Relationship between Sediment Transport Capacity and Water Discharge

Results show that Q_{sc_river} and Q_{sc_pool} increase with water discharge, Q_w, but differ in the threshold discharge for initial motion (Fig. 2). Rivers transport sediment when $\tau_* > \tau_{*c\_river}$, while sediment transport out of plunge pools requires a discharge that both moves sediment ($\tau_* > \tau_{*c\_pool}$) and suspends particles over the pool walls (Scheingross and Lamb, 2016). For deep pools, sediment export from the pool typically requires larger water discharges than needed for transport in adjacent river reaches (Fig. 2B). These different transport thresholds cause deep pools to aggrade at low water discharge when sediment is transported in rivers but cannot be evacuated from pools (Fig. 2B).

Increasing water discharge increases the river sediment transport capacity (Fig. 2). However, above the threshold for sediment transport out of pools, Q_{sc_pool} increases with discharge at a faster rate than Q_{sc_river} because the jet impinges with greater shear stress on the pool floor and because sediment suspension is driven by the upward return flow exiting the plunge pool (Fig. 2B). The return flow is faster for greater water discharges, as larger discharges produce wider waterfall jets, thereby forcing the return flow to pass through a smaller cross-sectional area. This combination results in a transition in pools from net aggradation ($Q_{sc\_river} > Q_{sc\_pool}$) at low flows to net degradation ($Q_{sc\_river} < Q_{sc\_pool}$) at high flows, with the water discharge at the transition point denoted as Q_{w_scour} (Fig. 2). For the scour regime ($Q_w > Q_{w\_scour}$), sediment transport out of the pool exceeds the capacity of the downstream river reach. This convergence of transport forces bar formation at the downstream pool boundary (e.g., Fig. 1), even though the discharge is far above the threshold for incipient sediment motion (Fig. 2).

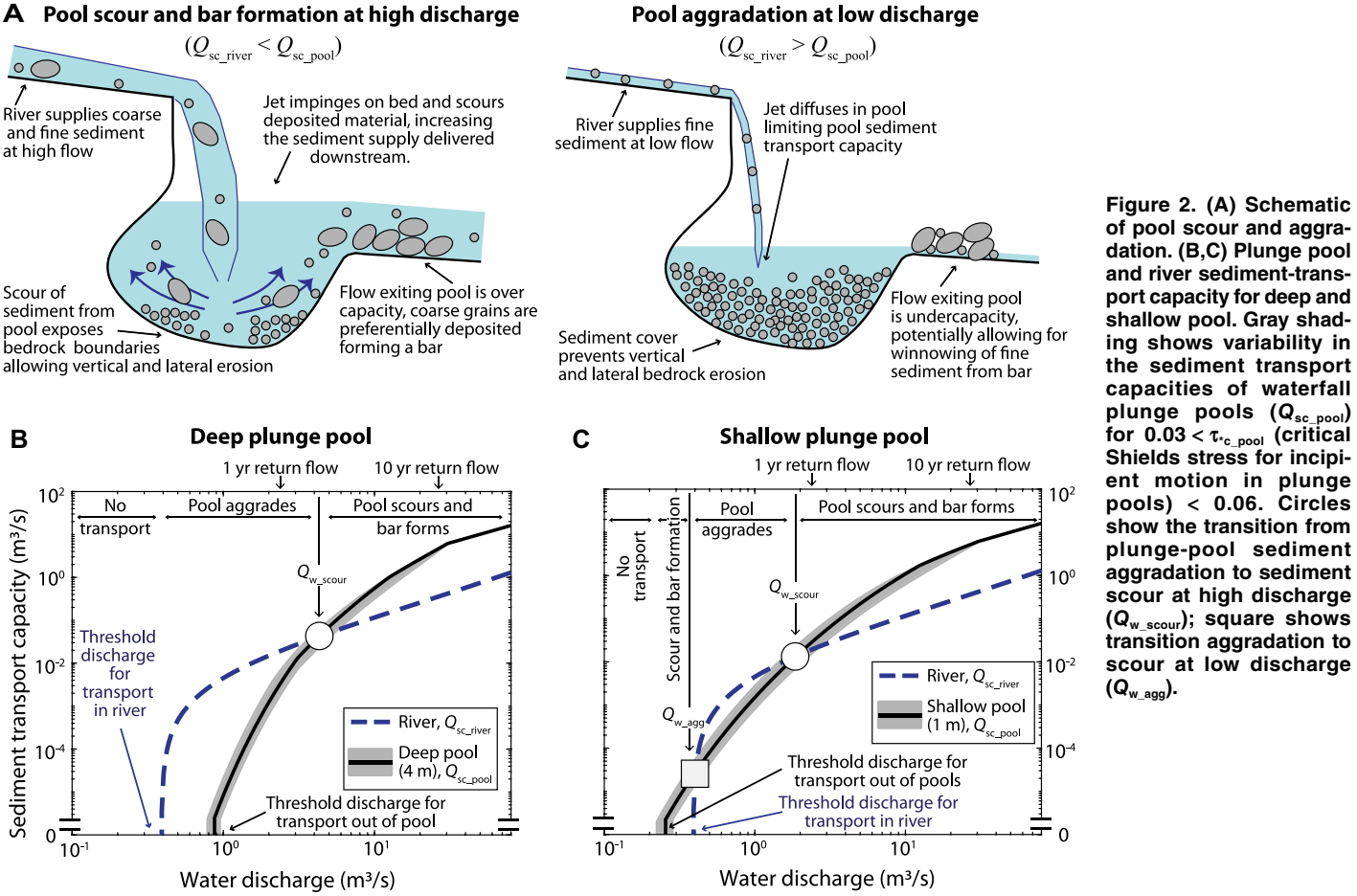

Figure 2. (A) Schematic of pool scour and aggradation. (B,C) Plunge pool and river sediment-transport capacity for deep and shallow pool. Gray shading shows variability in the sediment transport capacities of waterfall plunge pools (Q_{sc_pool}) for $0.03 < \tau^*_{c\_pool}$ (critical Shields stress for incipient motion in plunge pools) < 0.06. Circles show the transition from plunge-pool sediment aggradation to sediment scour at high discharge (Q_{w_scour}); square shows transition aggradation to scour at low discharge (Q_{w_agg}).

Plunge pool sediment transport capacity is highly sensitive to pool depth. For shallow pools (e.g., pools with alluvial fills), the threshold for transport out of the pool can correspond to a lower water discharge than the threshold for fluvial transport, resulting in a second regime of pool scour at low flows (Fig. 2C). This low-flow scour regime occurs because, for shallow pools, sediment is more easily suspended up and over the pool lip and because the jet experiences less drag before reaching the pool floor, resulting in higher stresses on the pool floor. This scour is transient, causing pools to deepen to the point where $Q_{sc\_river} = Q_{sc\_pool}$, and is common when pools fill with sand following wildfire (Fig. S2). We denote the discharge at the transition between the low-flow scour and pool aggradation regimes as Q_{w_agg}.

Influence of Varying Grain Size and Channel, Waterfall, and Pool Geometry

Changes in grain size and geometry of the channel, waterfall, and pool all can influence sediment transport capacity, thereby changing the magnitude of Q_{w_agg} and Q_{w_scour}. We solved for Q_{sc_pool} and Q_{sc_river} by systematically varying pool depth and radius, channel slope, grain diameter, and waterfall height while holding all other parameters constant (Fig. 3).

Channel slope exerts a large influence on river sediment transport but has negligible influence on plunge pool sediment transport (Fig. 3A). Therefore, plunge pools downstream of low-gradient channels can scour sediment at lower discharges because there is reduced sediment supply from upstream. As channel slope increases with all else held constant, rivers transport more sediment while the pool transport capacity stays approximately constant, requiring larger water discharges for pools to scour (Fig. 3A).

Increasing grain size decreases Q_{sc_river} and Q_{sc_pool} because larger grains require greater shear stresses (and thus greater discharges) for transport. This effect limits plunge pools more than rivers because increased settling velocities for large grains make them difficult to suspend out of deep pools. This results in plunge pools transitioning from scour to aggradation to no transport as grain size increases under constant water discharge (Fig. 3B). If water discharge and the transported grain size covary, as is common in nature, pools may maintain a state of scour or aggradation.

Variations in waterfall height and pool geometry influence Q_{sc_pool} but not Q_{sc_river}. Increasing waterfall height increases the jet velocity and thereby increases Q_{sc_pool}. This allows pools below taller waterfalls to transition from aggradation to scour at lower discharges than pools below shorter waterfalls (Fig. 3C). Deeper and wider pools have a lower sediment transport capacity because shear stress at the pool floor decreases with depth and it is more difficult to transport sediment over the pool walls as pools grow in depth and radius. This causes the transition from pool aggradation to scour to increase as pools deepen and widen, with all else held constant (Figs. 3D and 3E). At very shallow pool depths, pools can scour at low flows when transport in the river becomes negligible (Fig. 3D).

Relative Frequency of Plunge Pool Bedrock Erosion versus River Sediment Transport

To find the return period of floods capable of exposing and eroding the pool bedrock floor, we analyzed a preexisting database of 75 waterfalls (Scheingross and Lamb, 2016) and historical water discharge records (see the Supplemental Material). We calculated the conditions under which $Q_w > Q_{w\_scour}$ using a pool depth equal to the depth to bedrock. To account for potential sediment supply limitations, we varied the ratio Q_{s_river}/Q_{sc_river} from 0.1 to 1. While the onset of sediment motion in river channels occurred for floods with return periods <10 yr in 97% of the field examples analyzed, bedrock erosion in pools required larger floods with longer return periods (only 36%–53% of the surveyed pools, depending on Q_{s_river}/Q_{sc_river}, are predicted to erode in floods with return periods <10 yr) (Fig. 4; Fig. S3).

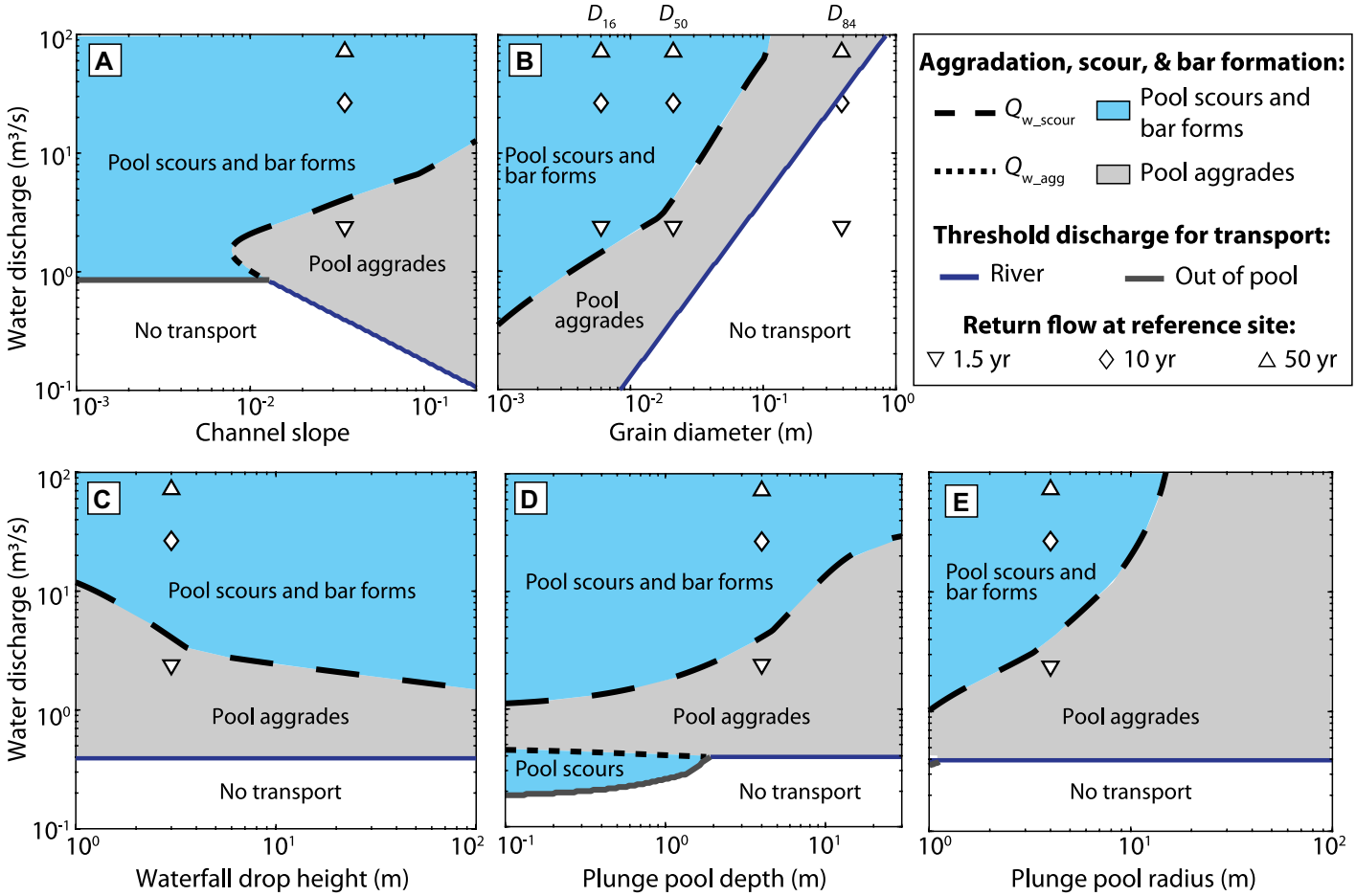

Figure 3. Phase space of pool scour and aggradation as function of channel slope (A), grain diameter (B), waterfall height (C), pool depth (D), and pool radius (E). Q_{w_scour} and Q_{w_agg} indicate the transition between plunge pool sediment scour and sediment aggradation regimes for high and low discharges, respectively. Calculations use Middle Switzer Falls reference site (California, USA) values and critical Shields stress for incipient motion in plunge pools (τ_{*c_pool}) = 0.045. D_{16}, D_{50}, and D_{84} represent grain diameters for which 16%, 50%, and 84% of the grain size distribution is finer, respectively.

DISCUSSION

Our theory provides a quantitative framework for modeling cycles of plunge pool sediment fill, scour, and bar formation, with implications for habitat, reconstructing past discharges, and landscape evolution. Isolating mechanistic controls on pool alluviation allows prediction of aquatic habitat availability associated with deep pools. For example, our work shows pools are more likely to fill after disturbances like wildfire and landsliding that can cause upland rivers to shift from supply- to transport-limited regimes, thereby increasing the sediment flux into pools. Similarly, prolonged low-flow periods may allow pools to remain within the aggradation regime for extended periods, causing pool aggradation and habitat loss during dry periods when ecosystems may already be stressed (Magoulick and Kobza, 2003) (Fig. 3).

Our work shows previous methods to estimate paleodischarge using the threshold of motion to form pool bars (e.g., Carling and Grodek, 1994) may underestimate the minimum bar-forming discharge (Fig. 2). This is because bars form when the mass flux of sediment at the downstream end of the pool exceeds the river's transport capacity (i.e., $Q_w > Q_{w\_scour}$), and these conditions are typically above the threshold of sediment motion in the river (Fig. 2). For example, for the case shown in Figure 2B, using the threshold of motion results in an ~10× lower estimate of the minimum bar-forming discharge relative to using Q_{w_scour}. Therefore, estimates of Q_{w_scour} (via measuring the grain size of bar deposits, in addition to waterfall and river geometry) may improve paleodischarge estimates relative to using the threshold of motion.

The large water discharges needed for pool bedrock erosion are greater than that required for

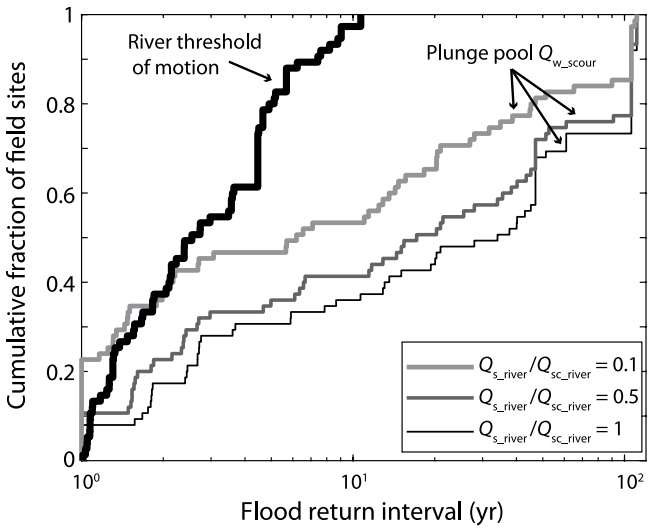

Figure 4. Comparison of flood return period for mobilizing sediment in river reaches ($\tau_* > \tau_{*c\_river}$; τ_*—Shields stress; τ_{*c_river}—critical Shields stress for incipient motion in the river channel) versus for scouring plunge pools to bedrock ($Q_w > Q_{w\_scour}$; Q_w—water discharge; Q_{w_scour}—water discharge at the transition point) for waterfalls surveyed by Scheingross and Lamb (2016). All calculations use τ_{*c_pool} = 0.045. Q_{s_river}—river sediment flux; Q_{sc_river}—river sediment transport capacity.

the onset of sediment transport in river reaches (the threshold commonly used to predict the onset of bedrock river incision; e.g., Tucker, 2004; Sklar and Dietrich, 2006; Scherler et al., 2017) (Fig. 4). While many waterfall erosion mechanisms exist, most mechanisms require erosion of exposed bedrock within the pool (e.g., Howard et al., 1994; Lamb et al., 2007; Scheingross et al., 2017) or transport of sediment away from the waterfall base (Gilbert, 1895; Lamb et al., 2006). Our results suggest that the threshold discharge for bedrock erosion is commonly greater for plunge pools than for adjacent river reaches (Fig. 4). These findings support the idea that waterfalls may erode at a different pace than river reaches (DiBiase et al., 2015), highlighting the likely importance of large, rare floods in knickpoint migration.

CONCLUSIONS

Our results show how mass-flux divergences—set by the difference between river and plunge pool sediment transport—control pool aggradation, scour, bar formation, and when waterfalls erode bedrock. At low water discharge, pools aggrade because the waterfall jet is too weak to penetrate the pool water and transport sediment at the rate it is supplied from upstream (Fig. 2). At high discharge, the waterfall jet impinges on the pool floor, and the high-velocity return flow within the pool causes Q_{sc_pool} to exceed Q_{sc_river}, sediment scour within the pool, and bar formation at the downstream pool margin (Fig. 2). The mass balance framework employed here explains observations of alluviated pools and downstream boulder bars (Fig. 1), provides a quantitative framework for predicting pool filling and constraining past discharges, and highlights waterfall erosion can occur during floods of different magnitude and frequency than bedrock erosion of lower-gradient river channels.

ACKNOWLEDGMENTS

We thank J. Prancevic and R. DiBiase for discussion, and five anonymous reviewers for comments. We acknowledge U.S. National Science Foundation (grant EAR-1147381 to M.P. Lamb and a Graduate Research Fellowship to J.S. Scheingross) and NASA (grant 12PGG120107 to M.P. Lamb) funding.

REFERENCES CITED

Buffington, J.M., and Montgomery, D.R., 1997, A systematic analysis of eight decades of incipient motion studies, with special reference to gravel-bedded rivers: Water Resources Research, v. 33, p. 1993–2029, https://doi.org/10.1029/96WR03190.

Carling, P.A., 1989, Hydrodynamic models of boulder berm deposition: Geomorphology, v. 2, p. 319–340, https://doi.org/10.1016/0169-555X(89)90018-4.

Carling, P.A., 1995, Flow-separation berms downstream of a hydraulic jump in a bedrock channel: Geomorphology, v. 11, p. 245–253, https://doi.org/10.1016/0169-555X(94)00052-S.

Carling, P.A., and Grodek, T., 1994, Indirect estimation of ungauged peak discharges in a bedrock channel with reference to design discharge selection: Hydrological Processes, v. 8, p. 497–511, https://doi.org/10.1002/hyp.3360080602.

DiBiase, R.A., Whipple, K.X., Lamb, M.P., and Heimsath, A.M., 2015, The role of waterfalls and knickzones in controlling the style and pace of landscape adjustment in the western San Gabriel Mountains, California: Geological Society of America Bulletin, v. 127, p. 539–559, https://doi.org/10.1130/B31113.1.

Finnegan, N.J., Sklar, L.S., and Fuller, T.K., 2007, Interplay of sediment supply, river incision, and channel morphology revealed by the transient evolution of an experimental bedrock channel: Journal of Geophysical Research, v. 112, F03S11, https://doi.org/10.1029/2006JF000569.

Gilbert, G.K., 1890, The history of the Niagara River: Extracted from the Sixth Annual Report to the Commissioners of the State Reservation at Niagara, for the year 1889: Albany, New York, James B. Lyon, Printer.

Gilbert, G.K., 1895, Niagara Falls and their history: National Geographic Monographs, v. 1, no. 7.

Griffiths, P.G., Webb, R.H., and Melis, T.S., 2004, Frequency and initiation of debris flows in Grand Canyon, Arizona: Journal of Geophysical Research, v. 109, F04002, https://doi.org/10.1029/2003JF000077.

Howard, A.D., Dietrich, W.E., and Seidl, M.A., 1994, Modeling fluvial erosion on regional to continental scales: Journal of Geophysical Research, v. 99, p. 13,971–13,986, https://doi.org/10.1029/94JB00744.

Keller, E.A., 1971, Areal sorting of bed-load material: The hypothesis of velocity reversal: Geological Society of America Bulletin, v. 82, p. 753–756, https://doi.org/10.1130/0016-7606(1971)82[753:ASOBMT]2.0.CO;2.

Lamb, M.P., Howard, A.D., Johnson, J., Whipple, K.X., Dietrich, W.E., and Perron, J.T., 2006, Can springs cut canyons into rock?: Journal of Geophysical Research, v. 111, E07002, https://doi.org/10.1029/2005JE002663.

Lamb, M.P., Howard, A.D., Dietrich, W.E., and Perron, J.T., 2007, Formation of amphitheater-headed valleys by waterfall erosion after large-scale slumping on Hawai'i: Geological Society of America Bulletin, v. 119, p. 805–822, https://doi.org/10.1130/B25986.1.

Lamb, M.P., Dietrich, W.E., and Sklar, L.S., 2008a, A model for fluvial bedrock incision by impacting suspended and bed load sediment: Journal of Geophysical Research, v. 113, F03025, https://doi.org/10.1029/2007JF000915.

Lamb, M.P., Dietrich, W.E., and Venditti, J.G., 2008b, Is the critical Shields stress for incipient sediment motion dependent on channel-bed slope?: Journal of Geophysical Research, v. 113, F02008, https://doi.org/10.1029/2007JF000831.

Lisle, T., 1979, A sorting mechanism for a riffle-pool sequence: Geological Society of America Bulletin, v. 90, p. 1142–1157, https://doi.org/10.1130/GSAB-P2-90-1142.

Magoulick, D.D., and Kobza, R.M., 2003, The role of refugia for fishes during drought: A review and synthesis: Freshwater Biology, v. 48, p. 1186–1198, https://doi.org/10.1046/j.1365-2427.2003.01089.x.

Mason, P.J., and Arumugam, K., 1985, Free jet scour below dams and flip buckets: Journal of Hydraulic Engineering, v. 111, p. 220–235, https://doi.org/10.1061/(ASCE)0733-9429(1985)111:2(220).

Nielsen, J.L., Lisle, T.E., and Ozaki, V., 1994, Thermally stratified pools and their use by steelhead in northern California streams: Transactions of the American Fisheries Society, v. 123, p. 613–626, https://doi.org/10.1577/1548-8659(1994)123<0613:TSPATU>2.3.CO;2.

Nott, J., and Price, D., 1994, Plunge pools and paleoprecipitation: Geology, v. 22, p. 1047–1050, https://doi.org/10.1130/0091-7613(1994)022<1047:PPAP>2.3.CO;2.

Nott, J.F., Price, D.M., and Bryant, E.A., 1996, A 30,000 year record of extreme floods in tropical Australia from relict plunge-pool deposits: Implications for future climate change: Geophysical Research Letters, v. 23, p. 379–382, https://doi.org/10.1029/96GL00262.

Pagliara, S., Hager, W.H., and Minor, H.E., 2006, Hydraulics of plane plunge pool scour: Journal of Hydraulic Engineering, v. 132, p. 450–461, https://doi.org/10.1061/(ASCE)0733-9429(2006)132:5(450).

Parker, G., 1990, Surface-based bedload transport relation for gravel rivers: Journal of Hydraulic Research, v. 28, p. 417–436, https://doi.org/10.1080/00221689009499058.

Pfeiffer, A.M., Finnegan, N.J., and Willenbring, J.K., 2017, Sediment supply controls equilibrium channel geometry in gravel rivers: Proceedings of the National Academy of Sciences of the United States of America, v. 114, p. 3346–3351, https://doi.org/10.1073/pnas.1612907114.

Phillips, C.B., and Jerolmack, D.J., 2016, Self-organization of river channels as a critical filter on climate signals: Science, v. 352, p. 694–697, https://doi.org/10.1126/science.aad3348.

Scheingross, J.S., and Lamb, M.P., 2016, Sediment transport through self-adjusting, bedrock-walled waterfall plunge pools: Journal of Geophysical Research: Earth Surface, v. 121, p. 939–963, https://doi.org/10.1002/2015JF003620.

Scheingross, J.S., and Lamb, M.P., 2017, A mechanistic model of plunge pool erosion into bedrock: Journal of Geophysical Research: Earth Surface, v. 122, p. 2079–2104, https://doi.org/10.1002/2017JF004195.

Scheingross, J.S., Lo, D.Y., and Lamb, M.P., 2017, Self-formed waterfall plunge pools in homogeneous rock: Geophysical Research Letters, v. 44, p. 200–208, https://doi.org/10.1002/2016GL071730.

Scheingross, J.S., Limaye, A.B., McCoy, S.W., and Whittaker, A.C., 2020, The shaping of erosional landscapes by internal dynamics: Nature Reviews: Earth and Environment, v. 1, p. 661–676, https://doi.org/10.1038/s43017-020-0096-0.

Scherler, D., DiBiase, R.A., Fisher, G.B., and Avouac, J.-P., 2017, Testing monsoonal controls on bedrock river incision in the Himalaya and Eastern Tibet with a stochastic-threshold stream power model: Journal of Geophysical Research: Earth Surface, v. 122, p. 1389–1429, https://doi.org/10.1002/2016JF004011.

Sklar, L.S., and Dietrich, W.E., 2006, The role of sediment in controlling steady-state bedrock channel slope: Implications of the saltation-abrasion incision model: Geomorphology, v. 82, p. 58–83, https://doi.org/10.1016/j.geomorph.2005.08.019.

Stein, O.R., Alonso, C.V., and Julien, P.Y., 1993, Mechanics of jet scour downstream of a headcut: Journal of Hydraulic Research, v. 31, p. 723–738, https://doi.org/10.1080/00221689309498814.

Tucker, G.E., 2004, Drainage basin sensitivity to tectonic and climatic forcing: Implications of a stochastic model for the role of entrainment and erosion thresholds: Earth Surface Processes and Landforms, v. 29, p. 185–205, https://doi.org/10.1002/esp.1020.

Wilcock, P.R., and Crowe, J.C., 2003, Surface-based transport model for mixed-size sediment: Journal of Hydraulic Engineering, v. 129, p. 120–128, https://doi.org/10.1061/(ASCE)0733-9429(2003)129:2(120).

Printed in USA

GSA Supplemental Information

Mass balance controls on sediment scour and bedrock erosion in waterfall plunge pools

J.S. Scheingross[1*] and M.P. Lamb[2]

[1]Deperatment of Geological Sciences and Engineering, University of Nevada Reno

[2]Division of Geological and Planetary Sciences, California Institute of Technology

*jscheingross@unr.edu

SUPPLEMENTAL INFORMATION

Flow hydraulics in channel reaches adjacent to waterfalls

We assume identical geometry of the reaches above and below the waterfall, as is common in narrow bedrock canyons, and steady, uniform flow such that

$$\tau_{river} = \rho g H S = \rho C_{f\_river} U^2 \quad \text{(S1)}$$

and

$$\tau_* = HS/RD \quad \text{(S2)}$$

Here, τ_{river} is the river shear stress, ρ is water density, g is gravitational acceleration, H is reach-averaged flow depth, S is the river slope, U is depth-averaged water velocity, R is the submerged sediment density (R=1.65 for quartz), D is the median grain size, and τ_* is the Shields stress. C_{f_river} is the river friction factor, which we solve for as (Garcia, 2008)

$$C_{f\_river} \equiv \left(\frac{u_*}{U}\right)^{1/2} = \left[8.1\left(\frac{H}{3D}\right)^{1/6}\right]^{-2} \quad \text{(S3)}$$

where $u_* = (\tau_{river}/\rho)^{1/2}$ is the shear velocity. We solve for H by combining equations (S1) and (S3) and assuming conservation of mass ($Q_w = UWH$, where W is channel width). This approach

ignores friction from the walls, which may be substantial for deep, narrow flows in bedrock canyons (e.g., Nelson and Seminara, 2011).

Waterfall plunge pool sediment transport capacity

We calculate the sediment transport capacity of waterfall plunge pools following Scheingross and Lamb (2016) which assumes steady, axisymmetric flow within a cylindrical plunge with vertical bedrock walls. The presence of vertical walls requires sediment to be suspended up and over the pools in order to be transported out of the pool. The model combines jet hydraulic theory and sediment suspension theory to predict the plunge pool sediment concentration under transport-limited conditions as

$$c(r,z) = c_b \exp\left(-\frac{(z - z_{mixed})}{L_d}\right)\left(\frac{I_0(r/L_d) + \frac{I_1(r/L_d)}{K_1(r/L_d)}K_o(r/L_d)}{I_0(\delta/L_d) + \frac{I_1(r/L_d)}{K_1(r/L_d)}K_0(\delta/L_d)}\right) \quad \text{(S4)}$$

where r and z are radial and vertical coordinates, respectively, c_b is the near bed sediment concentration that is solved for using standard sediment entrainment theory (Eq. 30 in Scheingross and Lamb (2016)), z_{mixed} is the height of the well-mixed layer of sediment near the pool floor and is assumed to be set by the height of sediment saltation following Sklar and Dietrich (2004), L_d parameterizes sediment mixing through a diffusive length scale which balances turbulence and particle settling, and δ is the radius of the region within the plunge pool in which flow is primarily downward due to advection from the descending jet. The notation I_0, K_0, I_1, and K_1 in Eq. (S4) denote modified Bessel functions of the first and second kind of order 0 and 1, respectively.

Plunge pool sediment transport capacity (Q_{sc_pool}) is predicted as

$$Q_{sc\_pool} = \frac{Q_w}{(z_{water} - z_{lip})} \int_{z=z_{lip}}^{z=z_{water}} c(r_{pool}, z)dz \quad \text{(S5)}$$

where z_{water} and z_{lip} are the elevation of the water surface and the plunge pool lip, respectively, and r_{pool} is the plunge pool radius. The Scheingross and Lamb (2016) theory shows that plunge pool sediment transport capacity can be predicted from four non-dimensional variables

$$\frac{Q_{sc\_pool}}{Q_w} = f\left(\frac{\tau_{*pool}}{\tau_{*c\_pool}}, \frac{(z_{lip} - z_{mixed})}{L_d}, \frac{r_{pool}}{L_d}, \frac{\delta}{L_d}\right) \quad \text{(S6)}$$

Where τ_{*pool} and τ_{*c_pool} are the Shields stress and critical Shields stress within the plunge pool, respectively. Scheingross and Lamb (2016) tested the theory against flume experiments and found good agreement across the range of these non-dimensional variables that are commonly observed in the field (see Figure 4 in Scheingross and Lamb (2016)).

The model of Scheingross and Lamb (2016) assumes that the waterfall jet falls a finite distance in freefall (i.e., the bedrock step composing the waterfall is emerged from the flow) and that the full waterfall jet enters the plunge pool. At very large discharges, these assumptions can be violated as the flow depth below the waterfall can exceed the waterfall drop height and the jet diameter can grow larger than that of the plunge pool. Under these cases, we refrain from predicting waterfall plunge pool sediment transport capacity.

River sediment transport capacity

We calculated river sediment transport capacity following Lamb et al (2008). This method calculates the total river sediment transport capacity, Q_{sc_river}, as the sum of the bedload and suspended load transport capacities, where suspended load transport capacity is calculated by integrating the product of the sediment concentration and velocity profiles. Following this method, river sediment transport capacity can be solved for by re-arranging Equation 20 from Lamb et al (2008)

$$Q_{sc\_river} = \frac{Q_{sc\_BL}(UH\chi + U_b H_b)}{U_b H_b} \quad \text{(S7)}$$

where Q_{sc_BL} is bedload transport capacity, U_b and H_b are the bedload velocity and height of the bedload layer, respectively, and χ is the integral that describes the vertical structure of the flow velocity and sediment concentration. We calculate the bedload transport capacity following Fernandez Luque and van Beek (1976)

$$Q_{sc\_BL} = 5.7(W)(RgD^3)^{0.5}(\tau_* - \tau_{*c})^{1.5} \quad \text{(S8)}$$

where τ_{*c} is the critical Shields stress for motion, and follow Lamb et al (2008) to calculate U, H, U_b,, H_b, and χ. Finally, we assumed channel width at a site is constant with varying discharge, as waterfalls often occur in steep-walled canyons.

Influence of grain size mixtures

Size-selective transport has yet to be examined in bedrock plunge pools; however, we expect that partial transport of fines during low flows in rivers (Hassan and Church, 2001; Scheingross et al., 2013) can explain the observations of plunge pools filled with fine sediment (Fig. 1 and S1). When the waterfall jet is weak, shear stress on the pool floor can be negligible, making pools traps of even the finest sediment. In contrast, mountain streams often transport a wide distribution of grain sizes during large floods (e.g., Rickenmann et al., 2012). Thus, size-selective transport may explain the observation of coarse bars at pool boundaries (Fig. 1 and S1), because bars form at high discharge capable of transporting coarse sediment, and size-selective disentrainment of sediment favors coarse grain deposition (Fedele and Paola, 2007). Fine sediment may also be winnowed from the bar during low flow when sediment transport is active in the river, but not the pool, which is further consistent with the existence of coarse sediment bars at the downstream pool boundary. For these reasons, we expect size-selective transport in the presence of sediment mixtures should yield similar results to our single grain size modeling.

The presence of sediment mixtures may also change the dynamics of sediment transport (e.g., Parker, 2008), as has been observed in alluvial scour pools where wider grain size distributions create deeper pools (Pagliara et al., 2006). Further investigation of how sediment mixtures influence the fill and scour of bedrock-walled plunge pools remains a key target for future work. However, if the observations of Pagliara et al. (2006) hold, they imply the presence of sediment mixtures would increase the discrepancy between plunge pool and river sediment transport capacity due to the increase in plunge pool depth, thereby accentuating the results presented here.

***Solving for* $\mathbf{Q_{w\_scour}}$**

We solve for the critical discharge necessary to scour sediment from plunge pools, Q_{w_scour}, numerically by finding the discharge for which $Q_{sc\_river}=Q_{sc\_pool}$ using estimates of the plunge pool geometry. We use particle size and the geometrics of the channel, waterfall and plunge pool to solve for Q_{sc_river} following Eq. (S7) and Q_{sc_pool} following Scheingross and Lamb (2016) for 500 logarithmically spaced water discharges between 10^{-1} and 10^{4} m^3/s. We then identify the water discharge for which $Q_{sc\_river}=Q_{sc\_pool}$ by finding the point of intersection between the Q_{sc_river}-discharge and Q_{sc_pool}-discharge curves. When using plunge pool bedrock geometry (i.e., the depth to the bedrock pool floor and the radius from the pool center to its bedrock sidewall), Q_{w_scour} represents the threshold discharge needed to scour all sediment from the pool, expose the bedrock bed, and allow for vertical bedrock incision via sediment impacts.

In some cases, the discharge needed for pools to scour to bedrock was so great that waterfalls became submerged and/or waterfall jets became wider than the plunge pools they fed into. These conditions violate the assumptions of the Scheingross and Lamb (2016), and we are unable to predict Q_{w_scour}. For these cases, we instead place a minimum bound on Q_{w_scour} using the maximum discharge at which the assumptions of the Q_{sc_pool} model has not been violated, and

for which $Q_{sc\_pool} < Q_{sc\_river}$ (Fig. S4). Figure 4 in the main text lumps both cases where Q_{w_scour} is directly calculated, and cases where a minimum estimate of Q_{w_scour} is made, thereby providing a conservative estimate of the return period necessary for waterfalls to scour to bedrock (that is, the lumping of these two metrics biases the results towards lower return periods). We explicitly separate these two cases in Figure S3 and Table S1.

Our calculation of the threshold discharge to allow bedrock erosion in plunge pools uses the field-surveyed waterfall height, plunge pool bedrock radius, channel geometry, and grain size reported in Scheingross and Lamb (2016). These pools typically had well-exposed bedrock walls allowing accurate measurements of plunge pool bedrock radii, but were often filled or partially-filled with sediment at the time of our surveying (including at the Middle Switzer Falls reference site), such that the true depth to bedrock is only known for 5 of the 75 waterfalls. For the remaining 70 waterfalls, we set pool depth equal to the pool bedrock radius for cases in which existing depth measurements were less than the radius. Experiments of plunge pool bedrock erosion suggest that waterfalls typically erode deep, narrow pools, with depths that can be greater than three times the plunge pool radius (Scheingross et al., 2017). Setting pool depth equal to pool radius is thus a purposely conservative estimate of the true depth, as this biases estimates of Q_{w_scour} for bedrock erosion towards lower discharges, and thus strengthens our argument that plunge pool bedrock erosion typically requires infrequent, large magnitude events (Fig. 4). Using the reported plunge pool depths in the Scheingross and Lamb (2016) database instead of the pool radii would still result in 44 of the 75 pools requiring floods with recurrence intervals greater than 10 y to scour below the maximum reported depth for conditions of $Q_{s\_river}/Q_{sc\_river} = 1$.

We determined the recurrence interval of flows large enough to erode bedrock in pools (or, in cases where the Scheingross and Lamb (2016) model assumptions were violated, the

minimum bound on Q_{w_scour} for bedrock erosion) by linearly interpolating along the discharge-frequency relations we created at each waterfall using historical water discharge records. We assumed a linear scaling between discharge and drainage area to account for the fact that gages and waterfalls were not co-located. When available, we used discharge records covering greater than 20 y from instrument gages on the same river as the waterfall of interest; where such records did not exist, we used records from nearby gages (Table S1). For cases where, the threshold discharge to erode bedrock exceeded the maximum discharge on record, and we set the recurrence interval equal to one year greater than the length of the discharge record (Table S1)

In some cases, the plunge pool sediment transport capacity was greater than the river sediment transport capacity across all discharges, there was no crossing of the plunge pool and river sediment transport capacity curves, and therefore no estimate of the threshold discharge for bedrock erosion. This behavior suggests disequilibrium plunge pool bedrock geometries, which may be a consequence of our conservatively low estimates for pool depth or indicate the presence of newly formed pools, and occurred for 6, 8, and 17 pools when setting Q_{s_river} / Q_{sc_river} equal to 1, 0.5, and 0.1, respectively. For an additional 17 plunge pools with Q_{s_river} / Q_{sc_river} equal to 1 (and 0 cases when Q_{s_river} / Q_{sc_river} was 0.5 or 0.1), curves crossed at two locations coinciding with Q_{w_agg} and Q_{w_scour} (e.g., Fig. 2C). For these cases, we calculated the threshold discharge for bedrock erosion at the higher crossing value (i.e, Q_{w_scour}). The lower crossing point (i.e., Q_{w_agg}) is typically coincident with the threshold discharge for sediment transport in adjacent river reaches (Fig. 2C); thus, even though pools have capacity to scour sediment at these low discharges, they lack upstream sediment supply, and hence have no or negligible availability of tools for bedrock erosion. In contrast, at discharges above Q_{w_scour}, there is both sediment supply and exposure of bedrock, allowing for efficient bedrock erosion.

SUPPLEMENTAL TABLES

We provide the Supplemental Tables at the end of this PDF to facilitate ease of reference and preservation. Supplemental tables are also provided in a separate file in .xlsx format for ease of access.

Table S1: Field-surveyed waterfall plunge pools from Scheingross and Lamb (2016).

Table S2: Individual clast measurements for grain size distributions shown in Figure 1.

REFERENCES CITED:

Chatanantavet, P., Whipple, K. X., Adams, M. A., and Lamb, M. P., 2013, Experimental study on coarse grain saltation dynamics in bedrock channels: Journal of Geophysical Research-Earth Surface, v. 118, no. 2, p. 1161-1176.

Fedele, J. J., and Paola, C., 2007, Similarity solutions for fluvial sediment fining by selective deposition: Journal of Geophysical Research-Earth Surface, v. 112, no. F2.

Ferguson, R. I., and Church, M., 2004, A simple universal equation for grain settling velocity: Journal of Sedimentary Research, v. 74, no. 6, p. 933-937.

Fernandez Luque, R., and van Beek, R., 1976, Erosion and transport of bed-load sediment: Journal of Hydraulic Research, v. 14, p. 127-144.

Garcia, M. H., 2008, Sediment transport and morphodynamics, *in* Garcia, M. H., ed., Sedimentation Engineering: Processes, Measurements, Modeling, and Practice: Reston, Virginia, American Society of Civil Engineers.

Graf, W. H., and Cellino, M., 2002, Suspension flows in open channels; experimental study: Journal of Hydraulic Research, v. 40, no. 4, p. 435-447.

Hassan, M. A., and Church, M., 2001, Sensitivity of bed load transport in Harris Creek: Seasonal and spatial variation over a cobble-gravel bar: Water Resources Research, v. 37, no. 3, p. 813-825.

Lamb, M. P., Dietrich, W. E., and Sklar, L. S., 2008, A model for fluvial bedrock incision by impacting suspended and bed load sediment: Journal of Geophysical Research-Earth Surface, v. 113, no. F3.

Nelson, P. A., and Seminara, G., 2011, Modeling the evolution of bedrock channel shape with erosion from saltating bed load: Geophysical Research Letters, v. 38.

Pagliara, S., Hager, W. H., and Minor, H. E., 2006, Hydraulics of plane plunge pool scour: Journal of Hydraulic Engineering-Asce, v. 132, no. 5, p. 450-461.

Parker, G., 2008, Transport of gravel and sediment mixtures, *in* Garcia, M. H., ed., Sedimentation Engineering: Processes, Measurements, Modeling, and Practice: Reston, Virginia, American Society of Civil Engineers.

Rickenmann, D., Turowski, J. M., Fritschi, B., Klaiber, A., and Ludwig, A., 2012, Bedload transport measurements at the Erlenbach stream with geophones and automated basket samplers: Earth Surface Processes and Landforms, v. 37, no. 9, p. 1000-1011.

Scheingross, J. S., Brun, F., Lo, D. Y., Omerdin, K., and Lamb, M. P., 2014, Experimental evidence for fluvial bedrock incision by suspended and bedload sediment: Geology, v. 42, no. 6, p. 523-526.

Scheingross, J. S., and Lamb, M. P., 2016, Sediment transport through self-adjusting, bedrock-walled waterfall plunge pools: J. Geophys. Res. Earth Surf., v. 121.

Scheingross, J. S., Lo, D. Y., and Lamb, M. P., 2017, Self-formed waterfall plunge pools in homogeneous rock: Geophysical Research Letters, v. 44, no. 1, p. 200-208.

Scheingross, J. S., Winchell, E. W., Lamb, M. P., and Dietrich, W. E., 2013, Influence of bed patchiness, slope, grain hiding, and form drag on gravel mobilization in very steep streams: Journal of Geophysical Research-Earth Surface, v. 118, no. 2, p. 982-1001.

Sklar, L. S., and Dietrich, W. E., 2004, A mechanistic model for river incision into bedrock by saltating bed load: Water Resources Research, v. 40, no. 6.

Figure S1: Waterfall plunge-pool systems with fine sediment fills and coarse sediment bars from the San Gabriel Mountains, CA with grain size distributions shown in Figure 1. Plunge pool 1 (A) and 2 (B) on Arroyo Seco. Large grains in foreground of (A) have a median diameter of ~20 cm for scale. (C) Wolfskill Falls, San Dimas Experimental Forest.

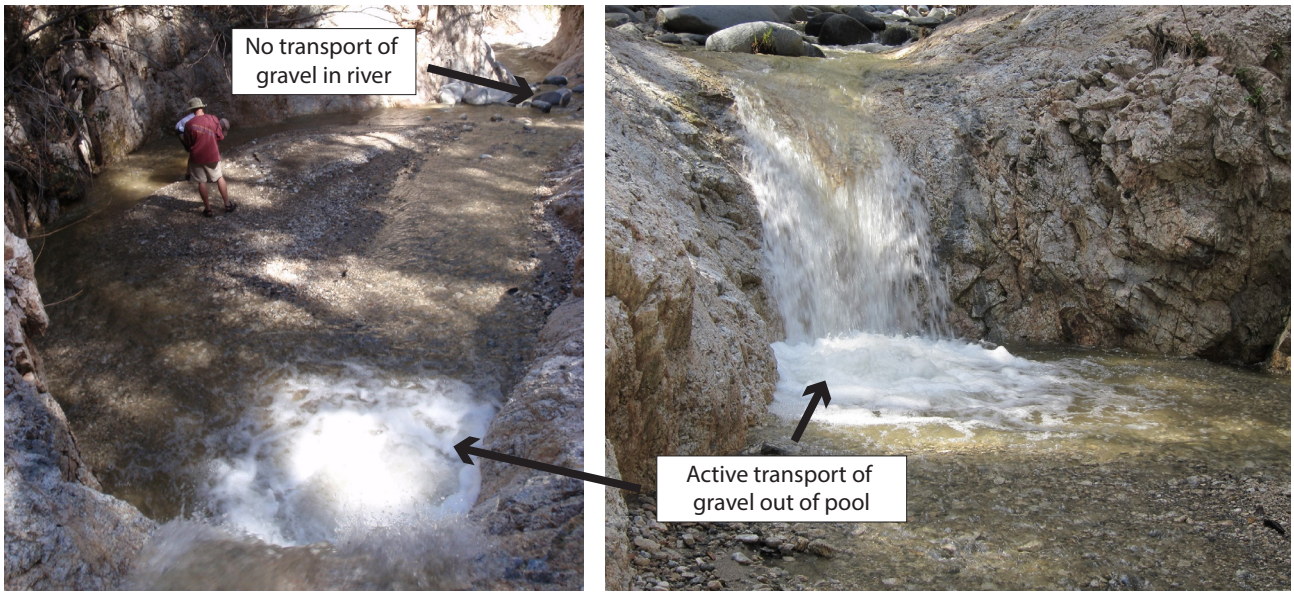

Figure S2: Example of waterfall plunge pool on Arroyo Seco, California. Photos taken in March 2010 and show the plunge pool filled with fine sediment following the Station Fire (August 2009). Field observations showed active transport of gravel out of the pool, but no gravel transport in the downstream river, consistent with our model predictions for shallow pools (Fig. 2C).

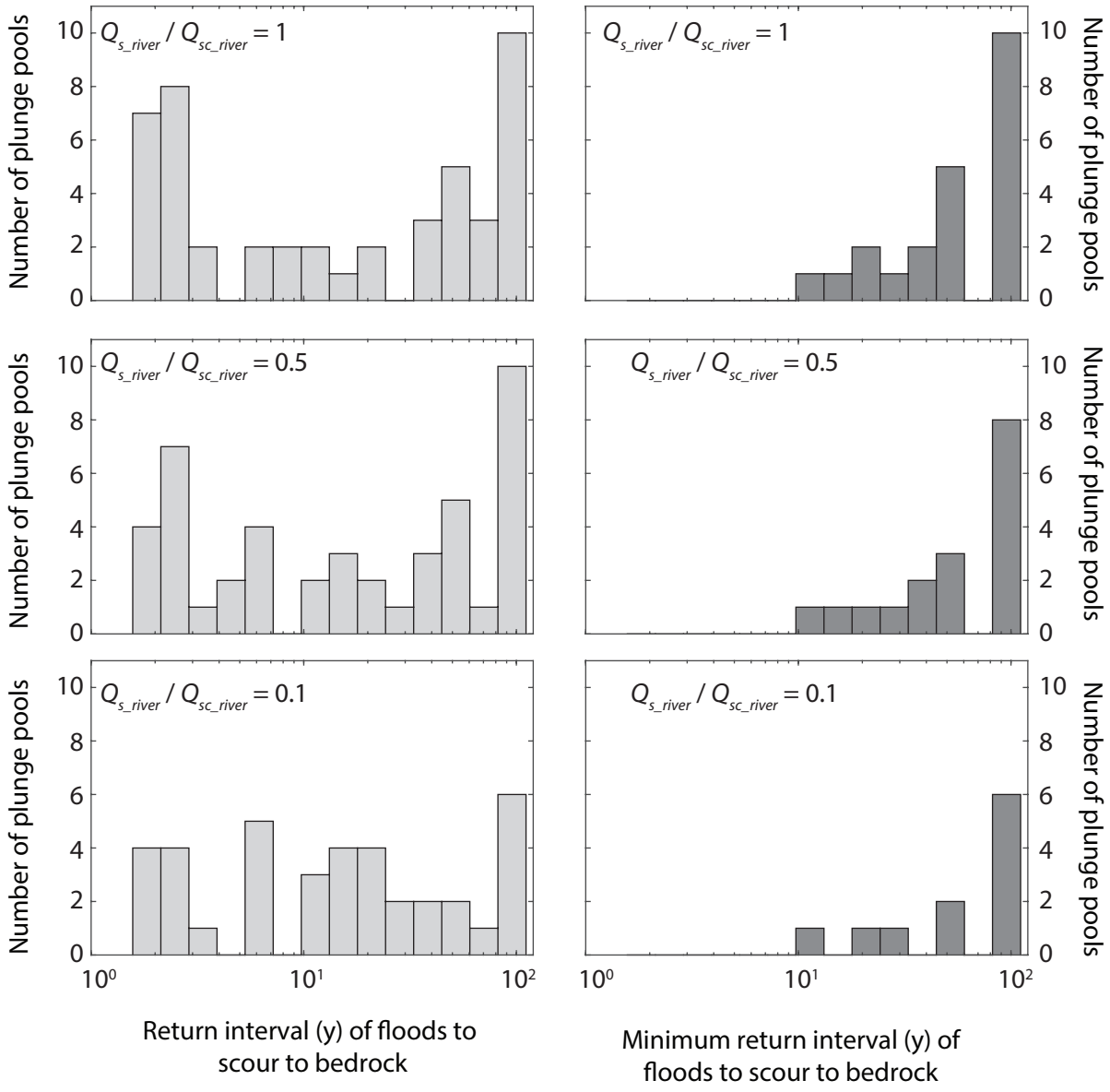

Figure S3: (Left column) Histogram of flood return interval for plunge pools in which the critical discharge to scour all sediment from pools and erode bedrock can be estimated. (Right column) Histogram of flood return interval for plunge pools where the waterfall becomes submerged prior to the onset of bedrock erosion. For these cases, we use the discharge of waterfall submergence as a minimum estimate of the threshold discharge to scour to bedrock. All calcluations use $\tau_{*c\_pool} = 0.045$, and we varied $Q_{s\_river} / Q_{sc\_river}$ from 0.1 to 1 as indicated in each panel. Historgrams omit cases in which is Q_{sc_pool} greater than Q_{sc_river} at all discharges, as these likely reflect disequilibrium plunge-pool geometries.

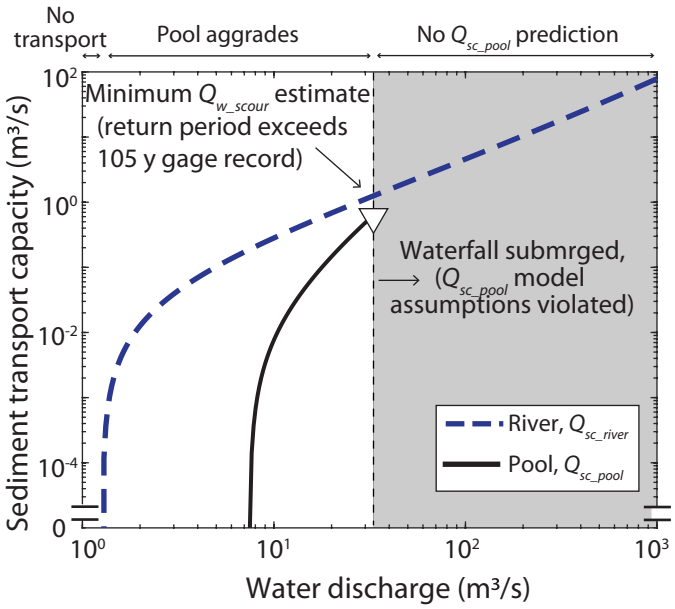

Figure S4: Example comparisons of river and plunge-pool sediment-transport capacities for a case where the waterfall becomes submerged before the pool is predicted to scour to bedrock, violating assumptions of the Scheingross and Lamb (2016) model (Waterfall DC2, Table S1). In this case, the discharge required to submerged the waterfall is ~4 times larger than the maximum, drainage-area scaled discharged predicted at this location using the 105 y gage record. Calcluations use $\tau_{*c\_pool} = 0.045$ and the values listed in Table S1.

Table S1. Field-surveyed waterfall plunge pools from Scheingross et al (2016)[†]

														Q_{s_river}/Q_{sc_river} = 1		Q_{s_river}/Q_{sc_river} = 0.5		Q_{s_river}/Q_{sc_river} = 0.1	
River	**ID**	***S***	***W* (m)**	***H*$_{drop}$ (m)**	***r*$_{pool}$ (m)**	***h*$_{pool}$ (m)**	***D*$_{50}$ river (m)**	***D*$_{84}$ river (m)**	***A* (km^2)**	**UTM East**	**UTM North**	**Pool floor**	**USGS Gage ID**	***A*$_{gage}$ (km^2)**	**Return period for bedrock ersoion (yr)**	***Q*$_{w\_scour}$ for bedrcok ersoion (m^3/s)**	**Return period for bedrock ersoion (yr)**	***Q*$_{w\_scour}$ for bedrcok ersoion (m^3/s)**	**Return period for bedrock ersoion (yr)**	***Q*$_{w\_scour}$ for bedrcok ersoion (m^3/s)**
Colby Canyon	CP1	0.06	5	2.5	2.3	0.9	0.15	0.38	2.62	395326	3792758	sed	11098000	41.40	106*	61**	106*	61.6**	106*	55.1
Colby Canyon	CP2a	0.07	4	2	0.9	0.65	0.15	0.38	1.64	395467	3792855	sed	11098000	41.40	106*	21.1**	106*	21.5**	106*	21.5**
Colby Canyon	CP2b	0.07	4	0.6	1.9	0.4	0.15	0.38	1.64	395467	3792855	sed	11098000	41.40	20	5.8**	20	5.7**	19.8	5.7**
Colby Canyon	CP3	0.06	3	1.2	1.8	0.5	0.15	0.38	1.64	395463	3792879	sed	11098000	41.40	106*	12.1**	106*	12.0**	106*	12.0**
Colby Canyon	CP4b	0.05	3	3.2	1.5	1	0.15	0.38	1.61	395568	3792957	sed	11098000	41.40	106*	53.1**	106*	51.1	106*	26.9
Colby Canyon	CP4c	0.05	3	1.9	2.3	1	0.15	0.38	1.61	395568	3792957	sed	11098000	41.40	106*	24.3**	106*	24.0**	106*	24.0**
Little Santa Anita	LR1	0.08	3.5	8.5	1.0	0.1	0.1	N/A	5.49	403678	3782944	sed	11100500	4.76	N/A[‡]	N/A[‡]	N/A[‡]	N/A[‡]	N/A[‡]	N/A[‡]
Little Santa Anita	LR2	0.08	5	4	2.9	0.5	0.1	N/A	5.49	403681	3782993	?	11100500	4.76	47*	44.8	47*	27.3	31.7	13.0
Little Santa Anita	LR3	0.08	4	3.5	0.7	0.3	0.1	N/A	5.54	403700	3782879	br	11100500	4.76	40	15.6**	41	15.9**	N/A[‡]	N/A[‡]
Little Santa Anita	LR4	0.08	5	8	2.0	1.5	0.1	N/A	5.55	403707	3782848	?	11100500	4.76	13	6.6	N/A[‡]	N/A[‡]	N/A[‡]	N/A[‡]
Little Santa Anita	LR5a	0.08	4	5.5	0.8	1.5	0.1	N/A	5.55	403704	3782825	?	11100500	4.76	N/A[‡]	15.6	N/A[‡]	N/A[‡]	N/A[‡]	N/A[‡]
Little Santa Anita	LR5b	0.08	4	1.25	1.3	1.5	0.1	N/A	5.55	403704	3782825	?	11100500	4.76	45	17.2**	45	17.2**	45.5	17.2**
Little Santa Anita	LD1a	0.08	5	1	0.6	0.24	0.1	N/A	5.59	403707	3782759	br	11100500	4.76	13	6.4**	13	6.4**	12.9	6.4**
Little Santa Anita	LD1b	0.08	5	4	0.7	0.1	0.1	N/A	5.59	403707	3782759	sed	11100500	4.76	34	13.9**	34	13.8**	N/A[‡]	N/A[‡]
Little Santa Anita	LR6	0.08	6	5.2	1.9	2	0.1	N/A	5.6	403719	3782712	?	11100500	4.76	47*	30.2	15	9.6	N/A[‡]	N/A[‡]
Little Santa Anita	LR7a	0.08	6	4.5	1.0	0.3	0.1	N/A	5.6	403675	3782679	sed	11100500	4.76	47*	36.7**	26	11.4	N/A[‡]	N/A[‡]
Little Santa Anita	LR7b	0.08	6	0.75	1.5	1.5	0.1	N/A	5.6	403675	3782679	?	11100500	4.76	28	12.1**	28	12.0**	27.6	12.0**
Little Santa Anita	LDF	0.1	6	1.5	2.1	0.1	0.1	N/A	5.7	403693	3782583	sed	11100500	4.76	47*	34.3**	47*	34.4**	47*	32.5
Little Santa Anita	LR8	0.11	6	4.5	2.0	0.1	0.1	N/A	5.72	403699	3782457	sed	11100500	4.76	47*	54.2	47*	21.3	12.4	5.9
Little Santa Anita	LR9	0.11	5	2.7	2.0	2	0.1	N/A	5.76	403722	3782369	?	11100500	4.76	47*	68.5**	47*	39.9	34.9	14.6
Little Santa Anita	LR10	0.09	3	3	1.5	1	0.1	N/A	5.8	403870	3782433	?	11100500	4.76	47*	37.5	47*	20.9	13.6	7.5
Little Santa Anita	LR11	0.09	2.5	4.7	2.3	4	0.1	N/A	5.82	403910	3782489	?	11100500	4.76	47*	19.8	38	15.8	14.7	9.1
Rubio Canyon	RR1	0.13	4	23	1.9	0.25	0.1	N/A	2.26	397227	3785825	sed	11098000	41.40	N/A[‡]	N/A[‡]	N/A[‡]	N/A[‡]	N/A[‡]	N/A[‡]
Rubio Canyon	RR2	0.13	3	6.5	1.6	0.2	0.1	N/A	2.26	397226	3785809	sed	11098000	41.40	106*	14.6	14	6.4	N/A[‡]	N/A[‡]
Rubio Canyon	RR3	0.13	4	4.6	1.5	0.1	0.1	N/A	2.27	397223	3787590	sed	11098000	41.40	106*	38.3	106*	15.5	7.1	3.5
Rubio Canyon	RR4	0.15	4	6.2	2.3	0.1	0.1	N/A	2.27	397178	3785777	sed	11098000	41.40	106*	26.3	106*	14.7	11.4	5.3
Rubio Canyon	RR5	0.15	3	7.5	2.0	0.1	0.1	N/A	2.27	397172	3785769	sed	11098000	41.40	106*	14.6	36	9.1	6.5	3.0
Rubio Canyon	RR6	0.18	4	8.5	1.4	0.1	0.1	N/A	2.28	397152	3785725	sed	11098000	41.40	38	9.6	6	2.9	N/A[‡]	N/A[‡]

Daisy Canyon	DC1	0.1	2	1.5	0.8	0.3	0.11	0.26	0.75	395633	3792897	sed	11098000	41.40	106*	11.3**	106*	11.4**	106*	11.4**
Daisy Canyon	DC2	0.1	3	2.3	1.3	0.65	0.11	0.26	0.75	395615	3792880	sed	11098000	41.40	106*	32.7**	106*	32.6**	106*	14.3
Daisy Canyon	DC3	0.1	2	1.1	1.0	0.5	0.11	0.26	0.76	395604	3792828	sed	11098000	41.40	106*	7.1**	106*	7.1**	106*	7.1**
Daisy Canyon	DC4	0.1	2	1.5	1.0	0.1	0.11	0.26	0.8	395581	3792807	sed	11098000	41.40	106*	11.3**	106*	11.4**	106*	11.4**
Daisy Canyon	DC5	0.1	2	4	1.0	0.1	0.11	0.26	0.85	395508	3792735	sed	11098000	41.40	106*	25.4	106*	12.7	20.3	3.0
Arroyo Seco	USF	0.035	5	12	7.3	0.5	0.021	0.32	12.08	393659	3791349	sed	11098000	41.40	4	9.7	3	7.4	1.9	4.7
Arroyo Seco (**Reference site**)	MSF	0.035	5	3	4.0	3	0.021	0.32	12.28	393855	3791207	?	11098000	41.40	2	4.3	2	3.2	1.5	2.1
Arroyo Seco	LSF	0.035	5	5	4.4	2	0.021	0.32	12.28	393855	3791207	?	11098000	41.40	2	3.7	2	2.9	1.5	2.0
Arroyo Seco	ASP1	0.014	4	1.21	3.0	0.3	0.021	0.32	12.53	394148	3790733	sed	11098000	41.40	2	4	2	2.9	1.3	1.6
Arroyo Seco	ASP2	0.049	3	1.45	3.0	0.5	0.021	0.32	12.51	394085	3790816	sed	11098000	41.40	2	5.9	2	4.5	1.5	2.4
Arroyo Seco	ASP3	0.052	5	2.18	3.0	0.3	0.021	0.32	12.49	394042	3790846	sed	11098000	41.40	2	4.3	2	3.0	1.3	1.5
Arroyo Seco	ASP4	0.035	5	2.32	3.0	3	0.021	0.32	12.49	394048	3790853	?	11098000	41.40	2	3.1	1	2.2	1.2	1.2
Arroyo Seco	ASP5	0.016	4	1.23	3.0	0.1	0.021	0.32	12.48	394066	3790866	sed	11098000	41.40	2	4.2	2	3.1	1.3	1.7
Fall Creek	FCR1	0.05	3	10.5	1.9	2	0.025	N/A	5.68	392877	3796770	?	11095500	275	3	0.6	2	0.5	N/A‡	N/A‡
Fall Creek	FCR2	0.05	4	12	3.7	0.7	0.025	N/A	5.68	392885	3796758	sed	11095500	275	11	2.9	7	2.2	5.7	1.3
Fall Creek	FCR3	0.05	3	7	3.9	0.55	0.025	N/A	5.68	392890	3796746	sed	11095500	275	14	4	11	3.0	6.2	1.8
Fall Creek	FCR4	0.05	4	23	3.9	0.5	0.025	N/A	5.68	392895	3796728	sed	11095500	275	9	2.8	7	2.1	5.7	1.3
Classic Canyon	CC1	0.12	4	1.5	1.5	0.4	0.05	N/A	1.42	392893	3796323	sed	11095500	275	61*	18.7	61*	10.3	38.7	4.4
Classic Canyon	CCR1	0.12	3	6.5	2.3	0.8	0.05	N/A	1.49	392684	3796459	sed	11095500	275	43	5.2	21	3.3	15.6	1.5
Classic Canyon	CCR2	0.12	3	9	2.3	0.5	0.05	N/A	1.49	392675	3796474	sed	11095500	275	20	3.2	17	2.1	14.3	1.2
Classic Canyon	CCR2a	0.12	3	2	1.4	1.3	0.05	N/A	1.49	392675	3796474	br	11095500	275	61*	11.3	44	5.3	18.3	2.5
Classic Canyon	CCR2b	0.12	3	2	1.6	0.3	0.05	N/A	1.49	392675	3796474	sed	11095500	275	61*	11.3	53	6.5	20.4	3.3
Fox Creek	FXR1	0.05	2	3	2.3	1	0.03	0.05	22.75	391431	3797425	br	11095500	275	2	1.9	2	1.3	1.4	0.5
Fox Creek	FXR2	0.05	5	13	3.5	0.75	0.03	0.05	22.75	391467	3797391	sed	11095500	275	3	2.6	2	2.0	2.0	1.2
Fox Creek	FXR3	0.05	3	3.5	3.5	1	0.03	0.05	22.75	391482	3797388	sed	11095500	275	6	6.1	5	4.4	2.7	2.5
Fox Creek	FXR4	0.05	3.6	7.5	3.4	0.85	0.03	0.05	22.75	391495	3797399	sed	11095500	275	3	2.9	3	2.2	2.2	1.4
Fox Creek	FXR5	0.05	4	3.5	2.8	0.7	0.03	0.05	22.75	391501	3797420	sed	11095500	275	4	3.6	3	2.5	2.2	1.3
Fox Creek	FXR6	0.05	7	27	2.0	0.5	0.03	0.05	22.75	391565	3797461	sed	11095500	275	N/A‡	N/A‡	N/A‡	N/A‡	N/A‡	N/A‡
Fox Creek	FXR7	0.05	4	6	3.0	2	0.03	0.05	22.75	391582	3797472	?	11095500	275	3	2.3	2	1.8	2.1	1.2
Fox Creek	FXR8	0.05	4	3.5	3.5	0.7	0.03	0.05	22.75	391611	3797487	sed	11095500	275	6	6	5	4.3	2.7	2.4
Fox Creek	FXR9	0.05	5	16	3.5	0.5	0.03	0.05	24.6	391524	3796514	sed	11095500	275	3	2.5	2	1.9	2.0	1.1
Millard Canyon	M1	0.075	5	17	2.9	0.3	0.05	N/A	5.1	394833	3787038	sed	11098000	41.40	2	2.4	2	1.7	N/A‡	N/A‡
Wolfskill Canyon	W1	0.1	6	9	5.0	1.2	0.17	0.13	5.2	430738	3781897	sed	N/A‡	5.40	8	113.5	6	80.6	3.1	36.4

Dry Meadow Ck	STC1	0.05	12	2.66	6.2	3.9	0.1	N/A	93.5	366139	3984275	?	11186000	2191	111*	147.1	111*	117.6	109.0	71.9
Dry Meadow Ck	STC2	0.05	12	3.74	4.8	2	0.1	N/A	93.5	366143	3984266	?	11186000	2191	111*	90.9	91	66.5	26.9	32.1
Dry Meadow Ck	STC3	0.05	12	5.34	9.2	5	0.1	N/A	93.5	366146	3984250	sed	11186000	2191	111*	170.9	111*	125.8	89.9	66.2
Dry Meadow Ck	STC4	0.05	12	3.89	5.9	4.62	0.1	N/A	93.5	366155	3984237	sed	11186000	2191	111*	113.9	111*	84.1	44.8	42.6
Dry Meadow Ck	STC5	0.05	12	1.24	4.9	2.21	0.1	N/A	93.5	366159	3984225	br	11186000	2191	51	50.7**	51	50.7**	51.3	50.7**
Dry Meadow Ck	STC6	0.05	12	2.85	7.4	2.53	0.1	N/A	93.5	366166	3984219	?	11186000	2191	111*	178.3	111*	141.7	111*	85.8
Dry Meadow Ck	STC7	0.05	12	2.36	4.5	2.55	0.1	N/A	93.5	366175	3984206	sed	11186000	2191	111*	133.7**	111*	101.4	65.1	58.8
Dry Meadow Ck	STC8	0.05	12	11	4.4	1.35	0.1	N/A	93.5	366191	3984207	?	11186000	2191	N/A‡	N/A‡	N/A‡	N/A‡	N/A‡	N/A‡
Dry Meadow Ck	STC9	0.05	12	13.99	6.4	3.57	0.1	N/A	93.5	366246	3984191	?	11186000	2191	19	23.2	12	14.4	N/A‡	N/A‡
Kapaa Stream	HFU	0.007	12	6	4.0	3	0.15	0.62	16.8	464537	2444738	?	16060000	61.50	N/A‡	N/A‡	N/A‡	N/A‡	N/A‡	N/A‡
SF Wailua River	WF	0.006	12	49	40.0	10	0.1	N/A	62	460951	2436662	?	16060000	61.50	2	358.1	2	300.6	1.3	213.8
Huleia Stream	KP	0.003	10	5.6	22.3	7.5	0.2	N/A	47	456876	2427414	?	16055000	46.83	15	414.2**	14	404.8**	11.0	367.7
Kaulaula Valley	KA	0.13	6	39	3.7	0.2	0.3	N/A	3.2	425986	2442220	?	16130000	9.81	N/A‡	N/A‡	N/A‡	N/A‡	N/A‡	N/A‡
Hanakapiai Stream	HF	0.4	10	120	22.0	4.7	0.3	N/A	4.5	438743	2453474	?	16115000	7.10	21*	40100**	21*	1630.1	21*	468.5

† S - reach-averaged channel slope, W - reach-averaged channel width upstream of the waterfall, H_{drop} - waterfall drop height, r_{pool} - plunge-pool radius, D_{50} and D_{84} - estimate of median and 84 percentile grain size for the river reach, respectively. Grain size data comes from a mix of visual estimates and pebble counts, in cases where pebble counts were performed, we report both D_{50} and D_{84}, for visual estimates, we report D50 only. h_{pool} - plunge pool depth (note: the "pool floor" column indicates if depth was to sediment, "sed", to bedrock, "br", or unknown, "?"), A and A_{gage} - drainage area at waterfall and discharge gaging station, respectively, Q_{w_scour} - Threshold discharge above which pools will scour to their bedrock floors.

* Recurrance interval of the threshold discharge for scour to bedrock was greater than the length of record at the gaging station and was set to the length of the record.

** Minimum estimate of the threshold discharge to scour to bedrock as the waterfall becomes submerged before the threshold discharge is reached.

⁑ 21-year discharge record for Wolfskill Falls from 1939-1959 provided by the US Forest Service.

‡ No value of Q_{w_scour} calculated as pool sediment transport capacity was greater than river sediment transport capacity for all discharges, likely indicating a disequilibrium bedrock geometry of the waterfall plunge pool.

Table S2: Individual clast measurements for grain size distributions shown in Figure 1*

Particle diameter (cm)							
Arroyo Seco					Wolfskill Falls		
Channel	Pool 1	Bar 1	Pool 2	Bar 2	Channel	Pool	Bar
48	1	8	0.1	40	20	2	10
6	1	9	0.1	22	4	0.8	8
50	0.5	48	0.3	13	24	1.8	28
17	2	85	3.2	35	1	1.5	20
46	1	3	1.5	6	2	1.5	3
0.6	1	4	4.5	0.1	3	4.5	4
222	2	1	7.5	75	20	4	25
1.7	4	20	1.2	8	2	3	21
0.3	2	45	11	1	3	0.1	15
9.3	4	44	4	13	10	2	16
1.2	2	66	5	45	3	1.5	18
2.1	6	45	10.5	0.1	0.5	1	16
1.6	2	85	0.1	0.1	2	0.1	10
0.6	1	8	2	0.1	10	0.1	20
0.6	2	35	10	90	1	0.8	25
0.8	0.6	70	21	0.1	2	20	16
2.4	2	30	2.5	0.1	1	0.9	12
0.7	0.3	6	4	40	1	1.2	12
0.9	3.5	23	0.1	2	20	0.4	26
4.1	0.8	15	2	2	23	1.1	23
4	4	30	0.8	2	2	0.5	17
30	2.5	4	13	1	3	70	26
120	1.2	3	3.5	0.1	2	1.5	22
0.6	7.5	15	0.5	2	2	0.5	14
47	2	30	5.5	4	5	0.1	19
1.6	1.2	0.1	2.5	110	4	0.1	10
1.1	1.8	20	0.1	25	2	0.1	12
1	0.5	12	1.1	17	1	0.1	6
4.2	0.3	11	5.5	35		0.1	10
42	0.5	55	3.5	45		0.1	27
3.1	0.8	0.5	2.1	0.1		8	11
1.4	0.3	3	0.1	0.1		0.1	28
1.6	3	6	0.1	45			32
0.9	2	45	2	0.1			27
2.1	0.1	28	1.5	0.1			18
43	0.6	80	0.1	0.1			7
4.9	0.3	0.5	5.5	0.1			25
8.8	4.5	0.1	5	42			10
7.6	1.2	4	6	3			13
2.1	2.5	0.5	1	70			7
2.2	6	2	0.5	42			7
3.2	2.5	50	4	10			22
2.6	1.5	30	0.5	0.1			30

0.6	2	35	0.2	65	17
0.4	2	60	1	0.1	8
1.2	0.3	2	2	3	15
0.3	0.5	4	0.1	70	30
2.7	1.2	38	0.2	8	15
0.8	1.5	22.1	2	30	11
1.1	0.2	41	0.1	90	12
2.1	0.1	2.5	5	5	17
4.5	0.1	50	1.5	55	10
5.1	2		8	5	16
4.1	0.5		5	0.1	19
3.2	1.2		1.5	50	18
0.5	0.2		4.5	0.1	15
0.9	0.2		1.5	0.1	24
0.5	1.5		7	50	18
0.5	2		2.5	0.2	13
4	0.1		2.5		12
18	1.2		7		11
52	0.1		1.5		6
0.2	2		0.1		
40	1.6		0.1		
80	1.2		0.1		
80	0.7		0.3		
4.2	4		2		
1.5	2.5		2		
2.2	1.5		5		
0.4	1.8		3.5		
1.6	2.5		4		
	1.3		2.5		
	1		0.5		
	2		1.5		
	1.5		8		
	0.8		2		
	1.2		1.5		
	1.5		3.5		
	0.1		1.5		
	0.1		5		
	1.2		0.7		
	0.5		1.1		
	0.2		2.6		
	2.2		1.2		
	0.3		8		
	0.5		5		
	1.5		1		
	0.5		2.5		
	0.1		1.5		
	0.1		0.1		

3.3	0.2	
1.5	0.4	
0.8	1.5	
1.5	4.2	
1.2	0.1	
1	0.1	
	0.1	
	0.1	

* All grain size measurements on Arroyo Seco and Wolfskill Falls made on 17 March 2010 and 12 March 2010, respectively . Grain size counts were conducted either by via a heel-toe random walk or stretching a measuring tape and measuring grains every 0.5 m. Arroyo Seco Pool/Bar 1 and Pool/Bar 2 are separated by less than 100 m and the channel grain size measurements was taken in the fluvial reach between the two waterfall plunge pools. At Wolfskill Falls the channel measurements were taken in a short (~ 3 m) section between the downstream bar and a subsequent dowstream waterfall, limiting the total number of grain size measurements.